7.4 EFFECTS OF HELIUM ATOMS ON THE STRENGTH OF BCC Fe GRAIN BOUNDARIES – Xiaoxun Zhang, Jiansha Ji, Fang Ma (Shanghai University of Engineering Science), G. R. Odette (University of California Santa Barbara), R. J. Kurtz, F. Gao (Pacific Northwest National Laboratory)

OBJECTIVE

The objective is to study the nucleation and growth of helium clusters at grain boundaries (GBs) and their effects on the cohesive strength of GBs in bcc Fe under uniaxial straining.

SUMMARY

The effects of helium atoms and the formation of helium clusters on Σ3 <110> {111}, Σ3 <110> {112} and Σ5 <100> {310} symmetric tilt GBs in bcc iron were studied by the molecular dynamics simulation method. We found that helium atoms are deeply trapped at the GBs during annealing at 300 K, and that two or more helium atoms aggregate to form a small helium clusters. The helium atom and small clusters act as a failure initiation site under uniaxial straining. We show that helium atoms decreases cohesive strength and ductility of all the grain boundaries in bcc Fe that were studied.

PROGRESS AND STATUS

Introduction

In fusion reactor environments helium decreases fracture toughness, creep rupture strength and promotes swelling [1]. However, the mechanisms and processes of helium effects are still not completely understood. There have been a large number of atomistic modeling studies of He in bulk bcc Fe [1-4]. On the other hand the literature on He atoms at Fe GBs is limited [5-9]. In the present study, the effects of helium atoms at various GBs are simulated under uniaxial straining using a new interatomic potential for Fe-He interactions, which is based on the electronic hybridization between Fe d-electrons and He s-electrons [10]. The migration of helium atoms and the formation of helium clusters on the Σ3 <110> {111}, Σ3 <110> {112} and Σ5 <100> {310} symmetric tilt GBs were investigated using molecular dynamics simulations. We found that two or more helium atoms aggregate to form small helium cluster and that the helium atoms and clusters decrease the cohesive strength and ductility of bcc Fe GBs.

Simulation Methods

The Fe-Fe potential developed by Ackland et al. [11], the He-He potential developed by Aziz et al. [12], and the Fe-He potential developed by Gao et al. [10] were combined and used in the present atomistic calculations. The supercells containing two grains of bcc Fe [13] are shown in Figure 1. The Σ3 <110> {111}, Σ3 <110> {112} and Σ5 <100> {310} symmetric tilt GBs were investigated to determine the cohesive strength of helium-loaded GBs under tensile deformation. The simulation cell sizes of Σ3 <110> {111}, Σ3 <110> {112} and Σ5 <100> {310} GBs were 21 Å × 110 Å × 21 Å, 20 Å × 112 Å × 21 Å and 20 Å × 110 Å × 18 Å, respectively. Periodic boundary conditions were imposed in the x and z directions, and uniaxial straining boundary conditions were applied along the y direction, where the x, y and z represent the [11-2], [111] and [1-10] directions in the Σ3 <110> {111} GB model, [1-11], [-112] and [-1-10] directions in the Σ3 <110> {112} GB model, and [031], [0-13] and [100] directions in the Σ5 <100> {310} GB model.

Different concentrations of helium atoms were inserted randomly around the GB plane (within 5 Fe layers on either side of the GB plane). The percentage of helium atoms was taken as a fraction of the Fe atoms within 5 layers near the GB plane. After the helium atoms were inserted, the system was quenched to 0 K, followed by a temperature rescaling to 300 K for 20 ps. Then, tensile displacement with a strain increment of 0.001 at each time step of one femto-second was applied to the atoms in the top and bottom regions of the model to drive the deformation of the simulation volume containing helium-loaded GBs.

The corresponding tensile stress and strain induced by the applied deformation were calculated as $\sigma = F/A_{xz}$ and $\varepsilon = (H - H_0)/H_0$, respectively, where F is the force acting in the y direction on the end plane, A_{xz} is the xz cross-section area of the model, H is the height of the model and H_0 is the initial height of the model. After each strain increment, energy minimization at 300 K was performed.

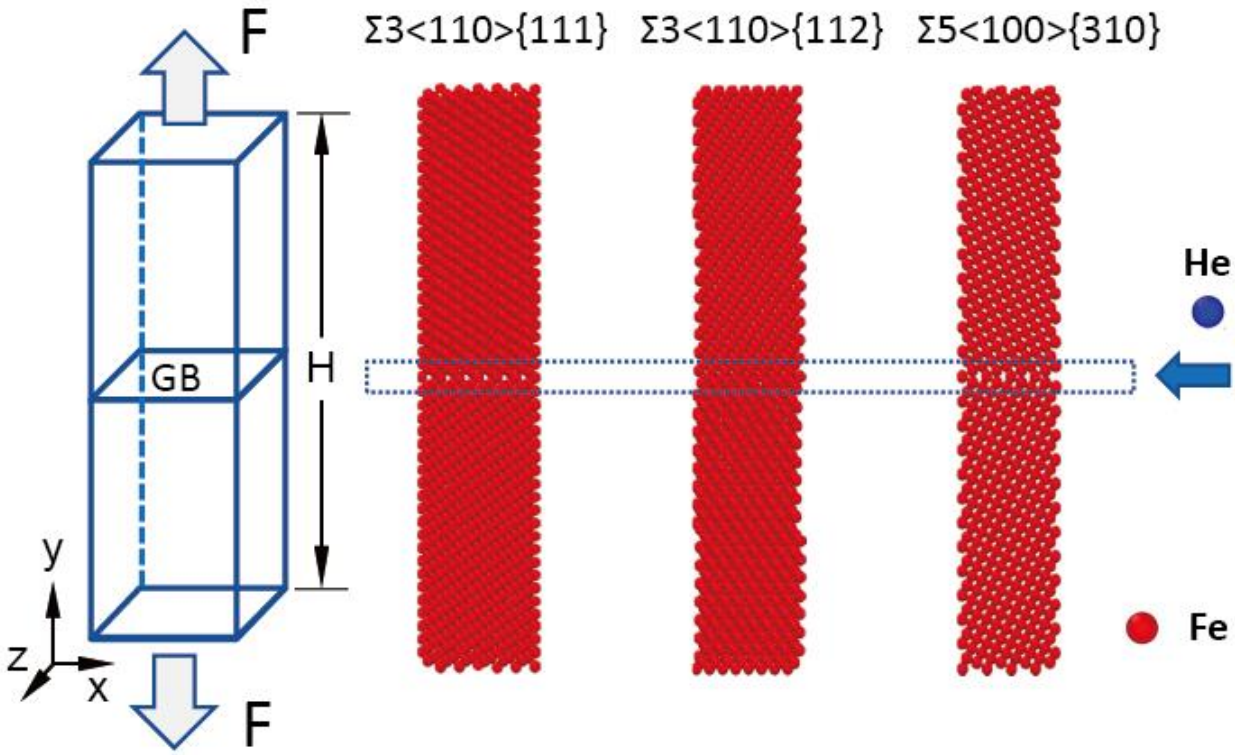

Figure 1. GB model under uniaxial load and different concentrations of helium atoms are inserted randomly around the GB plane (within 5 layers of Fe atoms)

Results

<u>Clusters formation during the annealing</u>

Helium atoms inserted interstitially into the nearby region, quickly move to and are trapped on the GB. Two or more helium atoms the aggregate to form small helium clusters. Figure 2a shows that twenty randomly helium atoms (10% He) migrate to form three helium clusters on the Σ3 <110> {112} GB at 300°K, with sizes of 5, 5, and 10, respectively. Figure 2b shows that twenty-four helium atoms (20% He) form three helium clusters on the Σ5 <100> {310} GB at 300 K, with sizes of 5, 9, and 10, respectively.

Evolution of helium clusters during uniaxial straining at 300°K

The GB helium atoms and small clusters act as a failure initiation sites. Figure 3a shows the failure initiation sites of 10% He loaded Σ3 <110> {111} GB at a strain of 0.0581. Figure 3b shows that that nucleation and propagation of a nano-crack occurred in the 5% He loaded Σ3 <110> {112} GB at a strain of 0.0974.

Figure 4 shows the evolution of helium clusters in a 10% He loaded Σ3 <110> {112} GB during uniaxial straining. Figure 4a shows that there are three isolated helium clusters A, B, and C 0 strain, and Figure 4b that cluster A approaches cluster B at a strain of 0.0357. Figure 4c shows that the three helium clusters connect since there are many nano-cracks produced (as displayed in Figure 3) just before the fracture of the GB (strain < 0.073). Finally, the three helium clusters aggregate to a large cluster just after the fracture of the GB (strain > 0.073).

Figure 5 shows the evolution of helium atoms and clusters in a 20% He loaded Σ5 <100> {310} GB. The number and distribution of the helium clusters in the Σ5 <100> {310} GB remain almost unchanged up to a just before the fracture at a strain of ≈ 0.049.

Effects of helium concentration on GB cohesive strength and ductility in bcc Fe

Figure 6 shows the stress-strain curves obtained for different GBs as a function of helium concentration. For clean GBs, the stresses increase linearly at the elastic regime followed by plastic deformation at constant stress in some GBs at higher strain. Fracture occurs when a second region of elastic strain reaches a critical value on the order of G/4 to G/3. The Σ3 <110> {112} and Σ5 <100> {310} clean GBs show extensive plastic deformation while the Σ3 <110> {111} clean GB does not exhibit an obvious yield point. The stress-strain curves for clean GBs presented here are very similar to those of Terentyev and He [14].

The presence of helium clusters in the GB results in a gradual decrease of the strength and ductility with increasing helium concentration. For example, GB loading of 0.68%, 4.8%, 10, and 20% helium in the Σ3 <110> {111} GB, results in a linear decrease in the fracture stress of 19.17, 15.80, 11.31 and 5.16 GPa, respectively. The corresponding maximum strains are 0.119, 0.096, 0.061, and 0.046, respectively (see Figure 6a). Notably, the curves are insensitive to the helium GB loading up to stresses and strains just before fracture. The fracture stresses and strains as a function of He loading are more clearly shown in Figures 7 and 8. The Σ3 <110> {111} is generally the weakest GB and suffers the largest fractional loss of strength at the highest helium loading, by a factor of 4. The drop in fracture strains in the GB is associated with fracture stresses that are less than needed for plastic yielding.

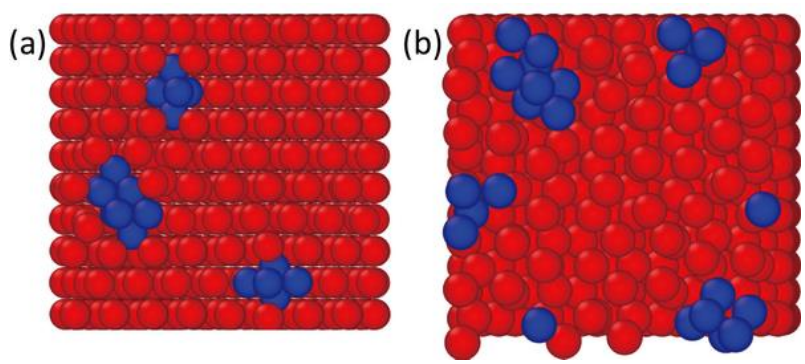

Figure 2. Helium atoms aggregate in small He clusters at 300 K of (a) 10% He loaded Σ3 <110> {112} GB and (b) 20% He loaded Σ5 <100> {310} GB in bcc Fe. (The red is Fe and the blue is He; the He atoms are drawn larger for clarity)

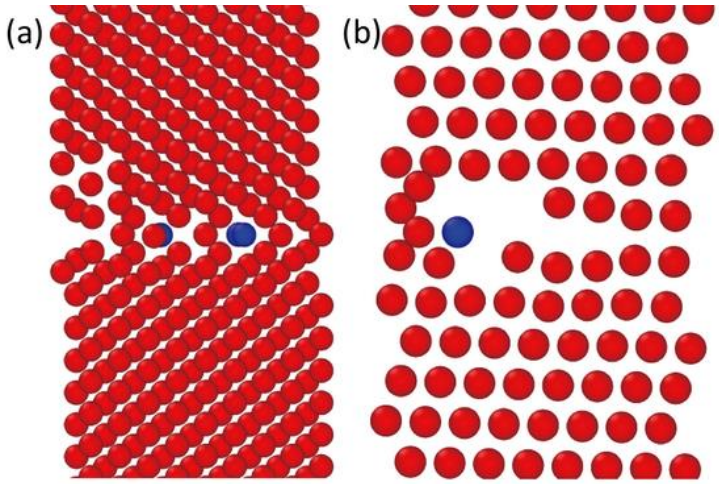

Figure 3. A single helium atom or small helium cluster at the grain boundary becomes a failure initiation site during the tensile loading:(a) 10% He loaded Σ3 <110> {111} GB at the strain of 0.0581 and (b) 5% He loaded Σ3 <110> {112} GB at the strain of 0.0974.

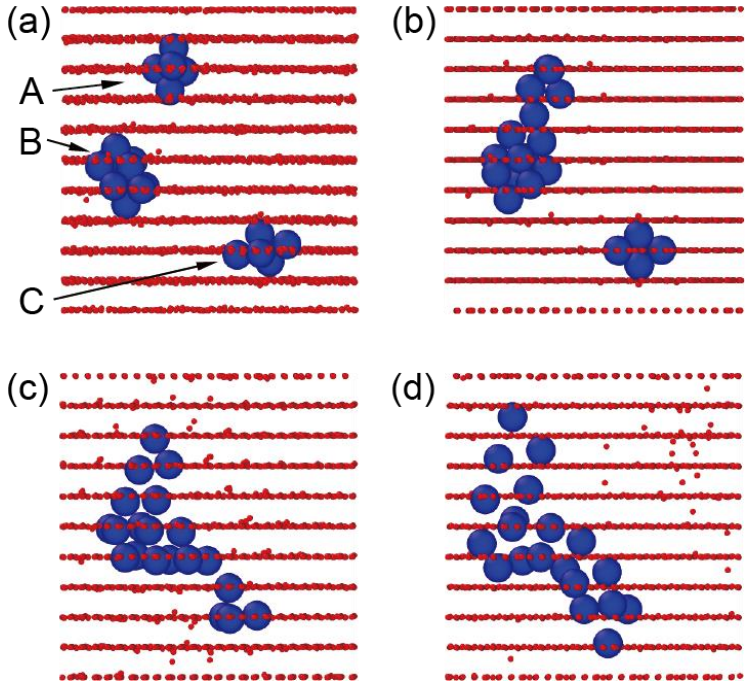

Figure 4. Evolution of helium clusters in a 10% He loaded Σ3 <110> {112} GB in bcc Fe during uniaxial straining to: (a) 0, (b) 0.0357, (c) just before fracture at 0.073), (d) just after fracture.

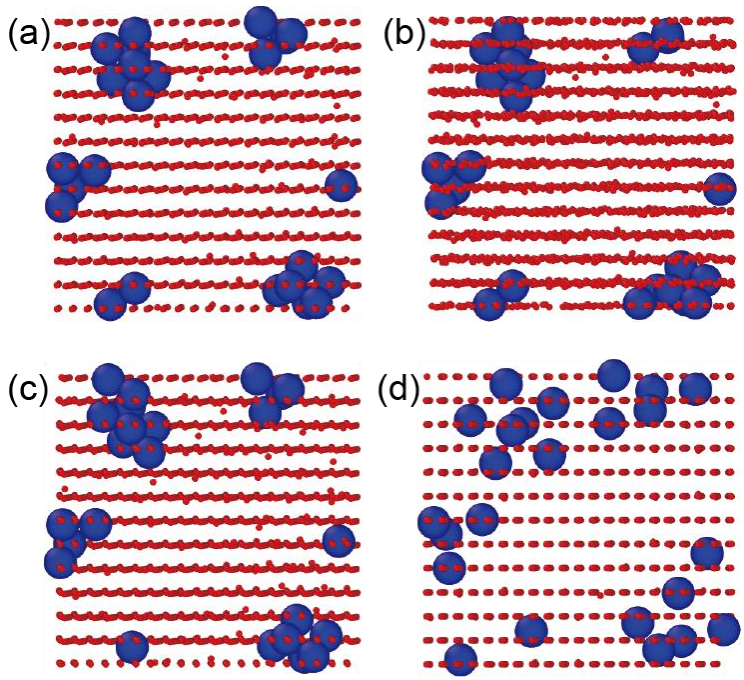

Figure 5. Evolution of helium clusters in a 20% He loaded Σ5 <100> {310} GB in bcc Fe during uniaxial straining to (a) 0, (b) 0.0189, (c) just before fracture at 0.049 and (d) just after fracture.

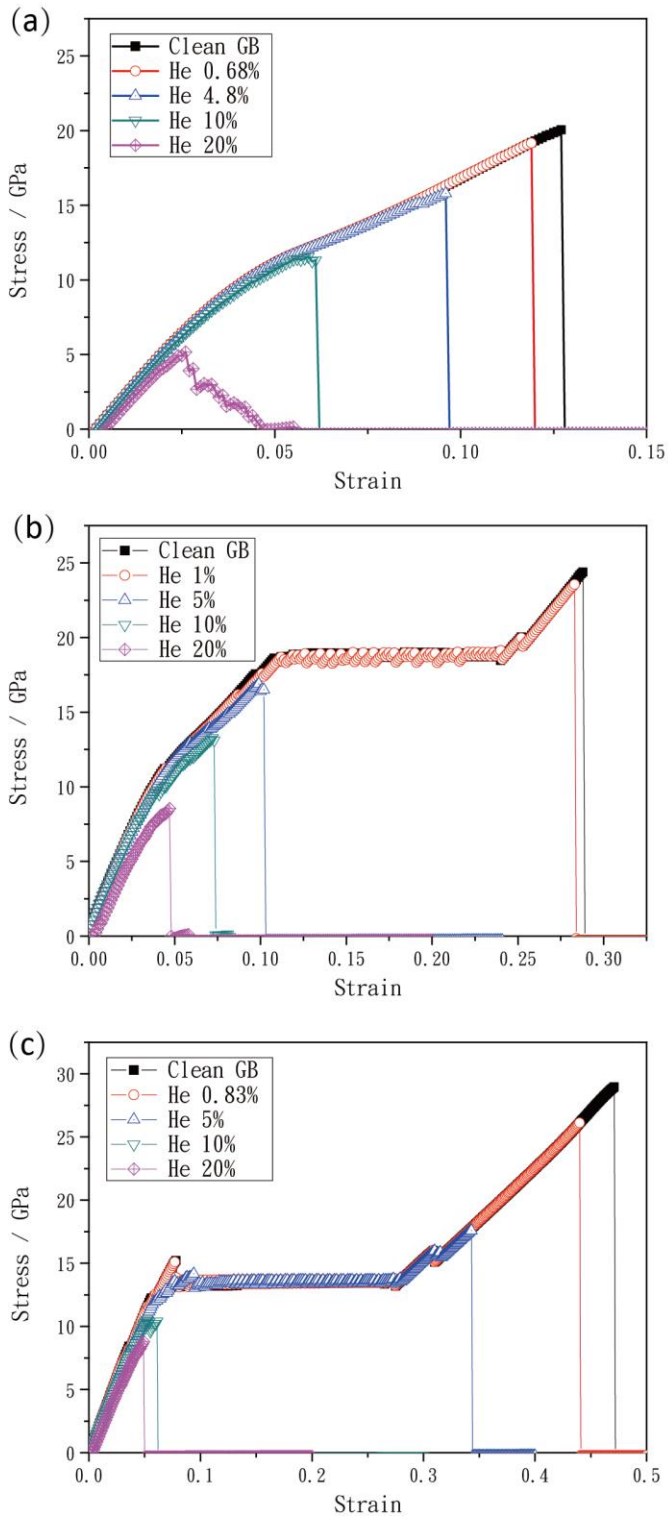

Figure 6. Stress-strain curves for the: (a) Σ3 <110> {111}, (b) Σ3 <110> {112}, and (c) Σ5 <100> {310} GB with different helium loadings.

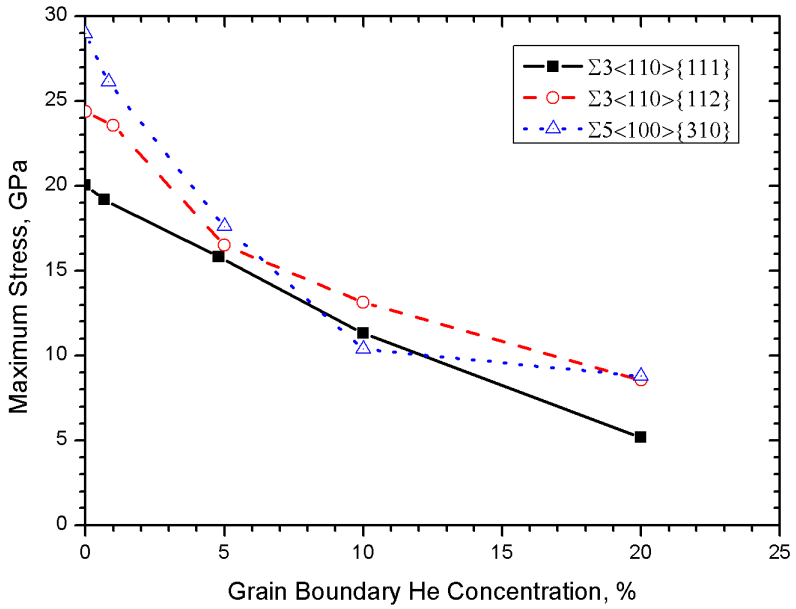

Figure 7. The effect of helium loading on the fracture stress of: Σ3 <110> {111}, Σ3 <110> {112} and Σ5 <100> {310} GB.

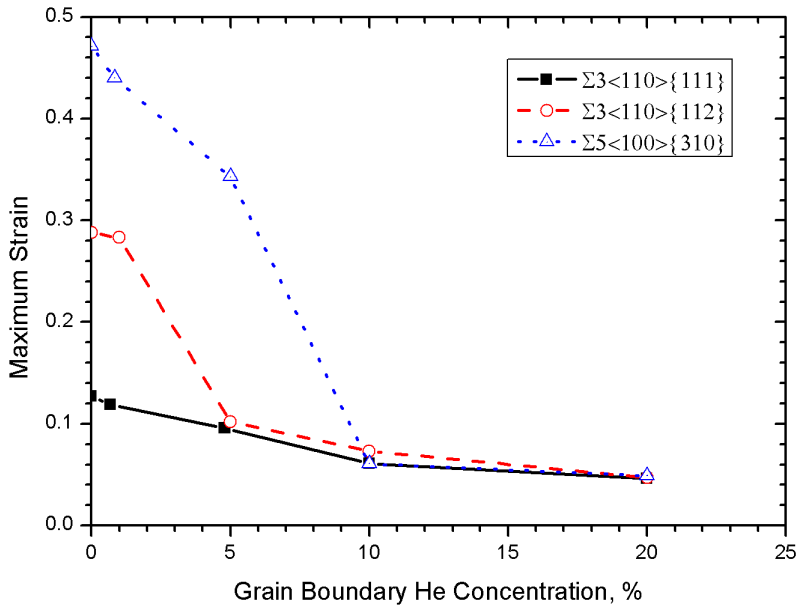

Figure 8. The effect of helium loading on the fracture strain of: Σ3 <110> {111}, Σ3 <110> {112} and Σ5 <100> {310} GB.

Discussion

Increasing loading of three special GB with helium results in large reductions in the fracture stress and strains of up to a maximum of ≈ 4 and 8, respectively. The reduction in strength is not associated with a uniform distribution of helium on the GB leading to a simple reduction of cohesive stress. Rather Helium introduced near GB is quickly trapped and forms clusters on the GB. Both helium atoms and especially small clusters act as sites for the formation and propagation of nano-cracks leading to GB fracture. Even at high helium loading the fracture stresses are very large with a minimum value of ≈ 5 GPa in the Σ3 <110> {111} GB. It is important to note that these results must be viewed as being qualitative and aimed at revealing phenomena rather than precise numbers. The simulations are affected by a variety of approximations compared to reality, including size, strain rate and use of simple many body potentials. Further, it will be important to explore the influence of other variables such as temperature, applied strain rate (including static vs. dynamic), hold periods and so on.

Acknowledgements

The lead author Professor Zhang was supported by SUES Innovation Project under grant 14KY0505 and supported by Science Foundation for the Youth Scholars of Shanghai Municipal Education Commission under Grant ZZGJD12081.

REFERENCES

[1] M. Samaras, Multiscale modelling: the role of helium in iron, Mater Today, 12(11), 46-53 (2009).
[2] S.J. Zinkle, Fusion materials science: Overview of challenges and recent progress, Phys. Plasmas, 12, 058101 (2005).
[3] M.J. Caturla, C.J. Ortiz, C.C. Fu, Helium and point defect accumulation: (ii) kinetic modeling, C. R. Phys., 9,(2008), 401-408.
[4] S.L. Dudarev et al., The EU programme for modelling radiation effects in fusion reactor materials: An overview of recent advances and future goals, J. Nucl. Mater., 386-388, (2009), 1-7.
[5] R.J. Kurtz, H.L. Heinisch, The effects of grain boundary structure on binding of He in Fe, J. Nucl. Mater., 329-333, (2004), 1199-1203.
[6] F. Gao, H.L. Heinisch, R.J. Kurtz, Diffusion of He interstitials in grain boundaries in α-Fe, J. Nucl. Mater., 351,(2006), 133-140.
[7] F. Gao, H.L. Heinisch, R.J. Kurtz, Migration of vacancies, He interstitials and He-vacancy clusters at grain boundaries in α-Fe, J. Nucl. Mater., 386-388, (2009), 390-394.
[8] Y. Zhang et al., First-principles study of helium effect in a ferromagnetic iron grain boundary: Energetics, site preference and segregation, Nucl. Instrum. Methods Phys. Res. B, 267, (2009), 3200-3203.
[9] T. Suzudo, H. Kaburaki, M. Yamaguchi, Modeling of the grain boundary segregation of helium in α-Fe, J. Nucl. Mater., 417, (2011), 1102-1105.
[10] F. Gao, Huiqiu Deng, H.L. Heinisch, R.J. Kurtz, A new Fe-He interatomic potential based on ab initio calculations in α-Fe, J. Nucl. Mater., 418, (2011) 115-120.
[11] G.J. Ackland, M.I. Mendelev, D.J. Srolovitz, S. Han, A.V. Barashev, Development of an interatomic potential for phosphorus impurities in α-iron, J. Phys.: Condens. Mater., 16, S2629 (2004).
[12] R.A. Aziz, A.R. Janzen, M.R. Moldover, Ab Initio Calculations for Helium: A Standard for Transport Property Measurements, Phys. Rev. Lett., 74, (1995), 1586.
[13] D. Terentyev, X. He, A. Serra, J. Kuriplach, Structure and strength of <110> tilt grain boundaries in bcc Fe: An atomistic study, Computational Materials Science, 49, (2010), 419-429.
[14] D. Terentyev,X. He, Effect of Cr precipitates and He bubbles on the strength of <110> tilt grain boundaries in BCC Fe: An atomistic study, Computational Materials Science, 50, (2011), 925-933.